

Sub-Nyquist Cyclostationary Detection for Cognitive Radio

Deborah Cohen, *Student IEEE* and Yonina C. Eldar, *Fellow IEEE*

Abstract—Cognitive Radio requires both efficient and reliable spectrum sensing of wideband signals. In order to cope with the sampling rate bottleneck when dealing with such signals, new sampling methods have been proposed that sample below the Nyquist rate. However, such techniques decrease the signal to noise ratio (SNR) due to aliasing effects, deteriorating the performance of the subsequent energy detection. Cyclostationary detection, which exploits the periodic property of communication signal statistics, absent in stationary noise, is a natural candidate for this setting. In this work, we consider cyclic spectrum recovery from sub-Nyquist samples, in order to achieve both efficiency and robustness to noise. We first show how the cyclic spectrum can be recovered directly from the low rate samples. Next, we derive a lower bound on the sampling rate required for perfect cyclic spectrum recovery in the presence of stationary noise. We show that even without any sparsity constraints on the signal, we can perfectly retrieve its cyclic spectrum from samples obtained below the Nyquist rate. Once the cyclic spectrum is reconstructed, we estimate the number of transmissions that compose the input signal, along with their carrier frequencies and bandwidths, that determine their support. To this end, we use parameter estimation techniques, that have previously been proposed in the Nyquist regime, on the cyclic spectrum recovered from sub-Nyquist samples. Simulations show that cyclostationary detection outperforms energy detection in low SNRs in the sub-Nyquist regime. This was already known in the Nyquist regime, but is even more pronounced at sub-Nyquist sampling rates.

I. INTRODUCTION

Spectrum sensing has been thoroughly investigated in the signal processing literature. Several sensing schemes have been proposed, with different performance and complexity levels. The simplest approach is energy detection [1], which does not require any a priori knowledge on the input signal. Unfortunately, energy detection is very sensitive to noise and performs poorly in low signal to noise ratio (SNR) regimes. In contrast, matched filter (MF) detection [2], [3], which correlates a known waveform with the input signal to detect the presence of a transmission, is the optimal linear filter for maximizing SNR in the presence of additive stochastic noise. This technique requires perfect knowledge of the potential received transmission. A compromise between both methods is cyclostationary detection [4]–[6]. This approach is more robust to noise than energy detection but at the same time only assumes the signal of interest exhibits cyclostationarity.

Cyclostationary processes have statistical characteristics that vary periodically, arising from the underlying data modulation mechanisms, such as carrier modulation, periodic keying or pulse modulation. The cyclic spectrum, a characteristic function of such processes, exhibits spectral peaks at certain frequency locations called cyclic frequencies, which are determined by the signal parameters, particularly the carrier frequency and symbol rate [6]. When determining the presence or the absence of a signal, cyclostationary detectors exploit one fundamental property of the cyclic spectrum: stationary noise and interference exhibit no spectral correlation [6]. This renders such detectors highly robust to noise.

The traditional task of spectrum sensing has recently been facing new challenges due, to a large extent, to cognitive radio (CR) applications [7]. Today, CRs are perceived as a potential solution to the spectrum over-crowdedness issues, bridging between its scarcity and its sparsity [8]. Even though most of the spectrum is already owned and new users can hardly find free frequency bands, various studies [9]–[11] have shown that it is typically significantly underutilized. CRs would allow secondary users to opportunistically use the licensed spectrum when the corresponding primary user (PU) is not active [7]. CR requirements dictate new challenges for its most crucial task, spectrum sensing and signal detection. On the one hand, spectrum sensing has to be performed in real time, efficiently and with minimal software and hardware resources. On the other hand, it has to be reliable and able to cope with low SNR regimes.

In order to efficiently sample sparse wideband signals, such as those CRs have to deal with, several new sampling methods have recently been proposed [12]–[15] that reduce the sampling rate in multiband settings below the Nyquist rate. The authors derive the minimal sampling rate allowing for perfect signal reconstruction in noise-free settings and provide specific sampling and recovery techniques. However, when the final goal is spectrum sensing and detection, reconstructing the original signal is unnecessary. Power spectrum reconstruction from sub-Nyquist samples is considered in [16]–[18]. All these approaches rely on energy detection. Unfortunately, the sensitivity of energy detection is amplified when performed on sub-Nyquist samples due to aliasing of the noise [19]. Therefore, this scheme fails to meet CR performance requirements in low SNR regimes. On the other hand, no a priori knowledge can be assumed on the received signals, making MF difficult to implement. Consequently, cyclostationary detection is a natural candidate for spectrum sensing from sub-Nyquist samples in low SNRs.

Signal detection using cyclostationarity and its application to spectrum sensing for CR systems in the Nyquist regime,

This project has received funding from the European Union's Horizon 2020 research and innovation program under grant agreement No. 646804-ERC-COG-BNYQ, and from the Israel Science Foundation under Grant no. 335/14. Deborah Cohen is grateful to the Azrieli Foundation for the award of an Azrieli Fellowship.

has been thoroughly investigated; see e.g., [5], [8], [20], [21]. Recently, cyclostationary detection from sub-Nyquist samples was treated in [22]–[30]. A general framework is adopted, that exploits a linear relation between the sub-Nyquist and Nyquist samples, over a finite sensing time. In particular, a transformation between the Nyquist cyclic spectrum and the time-varying correlations of the sub-Nyquist samples is derived to retrieve the former from the latter. In [22], the carrier frequencies, symbol periods and modulation types of the transmissions are assumed to be known. In this case, the cyclic spectrum can be reduced to its potential non zero cyclic frequencies, which are recovered using simple least squares (LS). However, this scheme cannot be applied in the context of blind spectrum sensing for CR.

The authors in [23], [24] consider low-pass compressive measurements of the correlation function. The cyclic autocorrelation is then reconstructed at a given lag using compressed sensing (CS) algorithms [31]. Two heuristic detection techniques are given in order to infer the presence or absence of a transmission. However, it is not clear how the signal itself should be sampled in order to obtain these correlation measurements. In addition, no requirements on the number of samples for recovering the cyclic autocorrelation or guarantees on the detection methods are provided.

In [25], [26], the authors consider a random linear relation between the autocorrelation of the sub-Nyquist samples and Nyquist cyclic spectrum and formulate a ℓ_1 -norm regularized LS problem, enforcing sparsity on the cyclic spectrum. The same ideas are adopted in [27] but the reconstruction is performed in matrix form, rather than vectorized, allowing for higher resolution. In [28], correlation lags beyond lag zero are exploited and the span of the random linear projections is extended beyond one period of cyclostationarity of the signal. These two extensions allow for simple LS recovery without any sparsity requirements on the signal.

The main drawback of this digital approach, adopted by all works above, is that it does not deal with the sampling scheme itself, since we do not have access to the Nyquist samples. It simply assumes that the sub-Nyquist samples can be expressed as random linear projections of the Nyquist samples. In addition, finite sensing time requires the assumption that the cyclic frequencies lie on a predefined grid. The theoretical resolution that can be achieved here is thus dictated by the sensing time, which is an inherent parameter of the sampling and reconstruction scheme, and not only a practical design parameter. Moreover, no theoretical guarantees on the minimal sampling rate allowing for perfect recovery of the cyclic spectrum have been given. A compression ratio bound is presented in [26] only for the special case of power spectrum recovery.

In [29], a concrete sampling scheme is considered, known as multicoset, or non-uniform sampling. The authors derive conditions on the system matrix to have full rank, allowing for perfect cyclic spectrum reconstruction from the compressive measurements. Random sampling in the form of a SAR-ADC architecture [32] is used in [30]. The resulting sampling matrix is identical to the multicoset sampling matrix, with the small distinction that the grid is that of the quantization time

rather than the Nyquist grid. While real sampling schemes are considered here, the theoretical cyclic spectrum resolution still depends on the sensing time, inherent to the sampling and recovery technique. The gridding, or discretization, is part of the theoretical derivations.

In this work, we propose to reconstruct the signal's cyclic spectrum from sub-Nyquist samples obtained using the sampling methods of [12]–[14]. Our theoretical approach does not involve any discretization or gridding and the cyclic spectrum can be recovered at any frequency. In addition, the MWC analog front-end presented in [13] is a practical sampling scheme that has been implemented in hardware [33]. We then perform cyclostationarity detection on the sub-Nyquist samples, thereby obtaining both an efficient, fast and frugal detector on the one hand and one that is reliable and robust to noise on the other. We derive a sampling rate bound allowing for perfect recovery of the cyclic spectrum in our settings, both for sparse and non sparse signals. We note that the cyclic spectrum can be perfectly recovered in the presence of stationary noise, from compressed samples, except for a limited number of cyclic frequencies that are multiples of the basic low sampling rate. For those, the reconstruction is performed in the presence of bounded noise.

We demonstrate that the cyclic spectrum of non sparse signals can be recovered from compressive samples, as shown in [28], [29] in the context of multicoset sampling. In particular, we show that, in the presence of stationary noise, the cyclic spectrum can be reconstructed from samples obtained at $4/5$ of the Nyquist rate, without any sparsity assumption on the signal. If the signal of interest is sparse, the sampling rate can be further reduced to $8/5$ of the Landau rate. Similar results were observed in [18] in the context of power spectrum reconstruction of stationary signals. There, it was shown that the power spectrum of non sparse signals can be retrieved at half the Nyquist rate and that of sparse signals can be perfectly recovered at the Landau rate. Here, we extend this result to cyclic spectrum reconstruction, which requires a higher rate. Once the cyclic spectrum is reconstructed, we apply our feature extraction algorithm, presented in [34] in the Nyquist regime, that estimates the number of transmissions and their respective carrier frequencies and bandwidths. Simulations show that cyclostationary detection outperforms energy detection in sub-Nyquist regimes, in low SNR.

This paper is organized as follows. In Section II, we describe the cyclostationary multiband model. Sections III and IV present the sub-Nyquist sampling stage and cyclic spectrum reconstruction algorithm and conditions, respectively. Numerical experiments are presented in Section V.

II. CYCLOSTATIONARY MULTIBAND MODEL

A. Multiband Model

Let $x(t)$ be a real-valued continuous-time signal, supported on $\mathcal{F} = [-1/2T_{\text{Nyq}}, +1/2T_{\text{Nyq}}]$ and composed of up to N_{sig} uncorrelated cyclostationary transmissions corrupted by

additive noise, such that

$$x(t) = \sum_{i=1}^{N_{\text{sig}}} s_i(t) + n(t). \quad (1)$$

Here $n(t)$ is a wide-sense stationary bandpass noise and $s_i(t)$ is a zero-mean cyclostationary bandpass process, as defined below, from the class of pulse-amplitude modulation (PAM) signals:

$$s_i(t) = \sqrt{2} \cos(2\pi f_i t) \sum_k a_{ik}^I g_i(t - kT_i) - \sqrt{2} \sin(2\pi f_i t) \sum_k a_{ik}^Q g_i(t - kT_i). \quad (2)$$

The unknown symbols modulating the in-phase and quadrature components are denoted $\{a_{ik}^I\}$ and $\{a_{ik}^Q\}$, respectively, and $g_i(t)$ are the unknown pulse shape functions. The single-sided bandwidth, the carrier frequency and the symbol period are denoted by B_i , f_i and T_i , respectively. Special cases of passband PAM include phase-shift keying (PSK), amplitude and phase modulation (AM-PM) and quadrature amplitude modulation (QAM) [35].

Formally, the Fourier transform of $x(t)$, defined by

$$X(f) = \lim_{T \rightarrow \infty} \frac{1}{\sqrt{T}} \int_{-T/2}^{T/2} x(t) e^{-j2\pi f t} dt, \quad (3)$$

is zero for every $f \notin \mathcal{F}$. We denote by $f_{\text{Nyq}} = 1/T_{\text{Nyq}}$ the Nyquist rate of $x(t)$. The number of transmissions N_{sig} , their carrier frequencies, bandwidths, symbol rates and modulations, including the symbols $\{a_{ik}\}$ and the pulse shape functions $g_i(t)$ are unknown, namely the reconstruction of the cyclic spectrum, defined in the next section, is performed in a blind scenario. The single-sided bandwidth of each transmission is only assumed to not exceed a known maximal bandwidth B , namely $B_i \leq B$ for all $1 \leq i \leq N_{\text{sig}}$. If the bandwidth is fully occupied, then it holds that $N_{\text{sig}}B$ is of the order of f_{Nyq} .

We will consider the special case of sparse multiband signals as well and show that the sampling rate for perfect cyclic spectrum reconstruction can be further reduced. In this setting, the number of transmissions N_{sig} which dictates the signal sparsity, or at least an upper bound on it, is assumed to be known and $N_{\text{sig}}B \ll f_{\text{Nyq}}$. We denote by $K = 2N_{\text{sig}}$ the upper bound on the number of occupied bands, to account for both the positive and negative frequency bands for each signal.

B. Cyclostationarity

A process $s(t)$ is said to be cyclostationary with period T_0 in the wide sense if its mean $\mathbb{E}[s(t)] = \mu_s(t)$ and autocorrelation $\mathbb{E}[s(t)s(t+\tau)] = R_s(t, \tau)$ are both periodic with period T_0 [4]:

$$\mu_s(t + T_0) = \mu_s(t), \quad R_s(t + T_0, \tau) = R_s(t, \tau). \quad (4)$$

Given a wide-sense cyclostationary random process, its autocorrelation $R_s(t, \tau)$ can be expanded in a Fourier series

$$R_s(t, \tau) = \sum_{\alpha} R_s^{\alpha}(\tau) e^{j2\pi\alpha t}, \quad (5)$$

where $\alpha = m/T_0$, $m \in \mathbb{Z}$ and the Fourier coefficients, referred to as cyclic autocorrelation functions, are given by

$$R_s^{\alpha}(\tau) = \frac{1}{T_0} \int_{-T_0/2}^{T_0/2} R_s(t, \tau) e^{-j2\pi\alpha t} dt. \quad (6)$$

The cyclic spectrum is obtained by taking the Fourier transform of (6) with respect to τ , namely

$$S_s^{\alpha}(f) = \int_{-\infty}^{\infty} R_s^{\alpha}(\tau) e^{-j2\pi f \tau} d\tau, \quad (7)$$

where α is referred to as the cyclic frequency and f is the angular frequency [4]. If there is more than one fundamental frequency T_0 , then the process $s(t)$ is said to be polycyclostationary in the wide sense. In this case, the cyclic spectrum contains harmonics (integer multiples) of each of the fundamental cyclic frequencies [6]. These cyclic frequencies are related to the transmissions carrier frequencies and symbol rates as well as modulation types.

An alternative interpretation of the cyclic spectrum, which we will exploit, expresses it as the cross-spectral density $S_s^{\alpha}(f) = S_{uv}(f)$ of two frequency-shifted versions of $s(t)$, $u(t)$ and $v(t)$, such that

$$u(t) \triangleq s(t) e^{-j\pi\alpha t}, \quad (8)$$

$$v(t) \triangleq s(t) e^{+j\pi\alpha t}. \quad (9)$$

Then, from [36], it holds that

$$S_s^{\alpha}(f) = S_{uv}(f) = \mathbb{E} \left[S \left(f + \frac{\alpha}{2} \right) S^* \left(f - \frac{\alpha}{2} \right) \right]. \quad (10)$$

The Fourier transform of a wide-sense stationary process $n(t)$ is nonstationary white noise and it holds that [36]

$$\mathbb{E} [N((f_1)N^*(f_2))] = S_n^0(f_1)\delta(f_1 - f_2). \quad (11)$$

Therefore, stationary noise exhibits no cyclic correlation [6], that is

$$S_n^{\alpha}(f) = 0, \quad \alpha \neq 0. \quad (12)$$

This property is the motivation for cyclostationary detection, in low SNR regimes in particular.

C. Cyclic Spectrum of Multiband Signals

Denote by $[f_i^{(1)}, f_i^{(2)}]$ the right-side support of the i th transmission $s_i(t)$. Then, $B_i = f_i^{(2)} - f_i^{(1)}$ and $f_i = (f_i^{(1)} + f_i^{(2)})/2$. The support region in the (f, α) plane of the cyclic spectrum $S_{s_i}^{\alpha}(f)$ of such a bandpass cyclostationary signal is composed of four diamonds, as shown in Fig. 1. More precisely, it holds that [6]

$$S_{s_i}^{\alpha}(f) = 0, \quad \text{for } \left| |f| - \frac{|\alpha|}{2} \right| \leq f_i^{(1)} \text{ or } |f| + \frac{|\alpha|}{2} \geq f_i^{(2)}. \quad (13)$$

Moreover, since $x(t)$ is bandlimited to \mathcal{F} , it follows that [6]

$$S_x^{\alpha}(f) = 0, \quad \text{for } |f| + \frac{|\alpha|}{2} \geq \frac{f_{\text{Nyq}}}{2}. \quad (14)$$

Since the transmissions $s_i(t)$ are assumed to be zero-mean and uncorrelated (coming from different sources), the cyclic

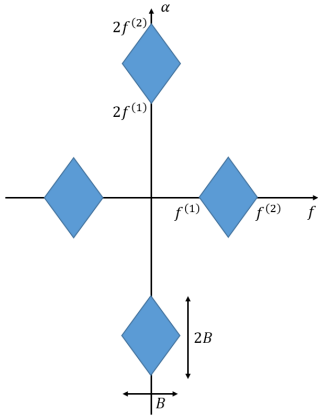


Fig. 1. Support region of the cyclic spectrum of $S_{s_i}^\alpha(f)$.

spectrum of $x(t)$ does not contain any additional harmonics which would result from correlation between different transmissions. The cyclic spectrum of $x(t)$ is thus given by

$$S_x^\alpha(f) = \begin{cases} \sum_{i=1}^{N_{\text{sig}}} S_{s_i}^\alpha(f) & \alpha \neq 0 \\ \sum_{i=1}^{N_{\text{sig}}} S_{s_i}^0(f) + S_n^0(f) & \alpha = 0. \end{cases} \quad (15)$$

At the cyclic frequency $\alpha = 0$, the cyclic spectrum reduces to the power spectrum and the occupied bandwidth along the angular frequency axis is $2N_{\text{sig}}B$, to account for both positive and negative frequency bands. This cyclic frequency $\alpha = 0$ contains the noise power spectrum as well. As a consequence, we choose to detect the transmissions and estimate their carriers and bandwidths at cyclic frequencies $\alpha \neq 0$. It follows from (15) that, besides the noise contribution at the cyclic frequency $\alpha = 0$, the support of $S_x^\alpha(f)$ is composed of $4N_{\text{sig}}$ diamonds, that is four diamonds for each transmission, as those shown in Fig. 1.

The support of $S_x^\alpha(f)$ is constituted by two types of correlations: the two diamonds lying on the angular frequency f axis and these lying on the cyclic frequency α . The diamonds lying on the f axis contains self-correlations between a band and its shifted version. These correspond to cyclic peaks at locations (f, α) , with $f \in \mathcal{F}$ and $0 \leq |\alpha| \leq B$. Cyclic features at these locations are the result of the transmissions symbol rate T_i . We note that the value of T_i can be derived from the bandwidth, as

$$T_i = \frac{1 + \gamma_i}{B_i}, \quad (16)$$

where $0 \leq \gamma_i \leq 1$ is the unknown excess-bandwidth parameter of $g_i(t)$ [35]. Therefore, cyclic peaks that stem from the symbol rate appear at cyclic frequencies $\alpha = \frac{1}{T_i} \leq B_i \leq B$.

The two diamonds lying on the α axis contain cross-correlations between two symmetric bands, belonging to the same transmission. These correspond to cyclic peaks at locations (f, α) , with $0 \leq |f| \leq B/2$ and $B < |\alpha| \leq f_{\text{Nyq}}$. In particular, applying (10) for $\alpha = \pm 2f_i$, namely

$$S_x^{\pm 2f_i}(f) = \mathbb{E}[X(f + f_i)X^*(f - f_i)], \quad (17)$$

computes the correlation between the positive and negative bands of the i th transmission. This generates a peak, or cyclic feature, in the cyclic spectrum at the location $(f = 0, \alpha = \pm 2f_i)$. By detecting the peak location, we can estimate the carrier frequency of the corresponding transmission $s_i(t)$. Furthermore, from (13), it is clear that the occupied bandwidth in the cyclic spectrum at $\alpha = \pm 2f_i$ is equal to the bandwidth B_i . These observations are the key to estimate the transmissions carrier frequency and bandwidth.

D. Goal

Our objective is to reconstruct $S_x^\alpha(f)$ from sub-Nyquist samples without any *a priori* knowledge on the support and modulations of $s_i(t)$, $1 \leq i \leq N_{\text{sig}}$. We find that the cyclic spectrum of non sparse signals can be recovered from samples obtained at $4/5$ of the Nyquist rate and if the signal is assumed to be sparse, the sampling rate can then be as low at $8/5$ of the Landau rate.

We then aim at estimating the number of transmissions N_{sig} present in $x(t)$, their carrier frequencies f_i and their bandwidths B_i . Once the signals' carrier frequency and bandwidth are estimated, the occupied support is entirely determined. In [34], we proposed a generic feature extraction algorithm for the estimation of N_{sig} , f_i and B_i , for all $1 \leq i \leq N_{\text{sig}}$, from the cyclic spectrum obtained from Nyquist samples. Here, we apply the same scheme to the reconstructed cyclic spectrum from sub-Nyquist rather than Nyquist samples.

III. SUB-NYQUIST SAMPLING

In this section, we briefly describe the sub-Nyquist sampling schemes we adopt. We consider two different sampling methods: multicoset sampling [12], [37] and the MWC [13] which were previously proposed for sparse multiband signals in conjunction with energy detection. We show that both techniques lead to identical expressions of the signal cyclic spectrum in terms of correlations between the samples. Therefore, the cyclic spectrum reconstruction stage presented in Section IV can be applied to either of the samples.

A. Multicoset sampling

Multicoset sampling [37] can be described as the selection of certain samples from the uniform grid. More precisely, the uniform grid is divided into blocks of N consecutive samples, from which only M are kept. The i th sampling sequence is defined as

$$x_{c_i}[n] = \begin{cases} x(nT_{\text{Nyq}}), & n = mN + c_i, m \in \mathbb{Z} \\ 0, & \text{otherwise,} \end{cases} \quad (18)$$

where $0 < c_1 < c_2 < \dots < c_M < N - 1$. Let $f_s = \frac{1}{NT_{\text{Nyq}}} \geq B$ be the sampling rate of each channel and $\mathcal{F}_s = [0, f_s]$. Following the derivations from multicoset sampling [12], we obtain

$$\mathbf{z}(\tilde{f}) = \mathbf{A}\mathbf{x}(\tilde{f}), \quad \tilde{f} \in \mathcal{F}_s, \quad (19)$$

where $\mathbf{z}_i(\tilde{f}) = X_{c_i}(e^{j2\pi\tilde{f}T_{\text{Nyq}}})$, $0 \leq i \leq M-1$, are the discrete-time Fourier transforms (DTFTs) of the multicoset samples and

$$\mathbf{x}_k(\tilde{f}) = X\left(\tilde{f} + K_k f_s\right), \quad 1 \leq k \leq N, \quad (20)$$

where $K_k = k - \frac{N+1}{2}$, $1 \leq k \leq N$ for odd N and $K_k = k - \frac{N+2}{2}$, $1 \leq k \leq N$ for even N . Each entry of $\mathbf{x}(f)$ is referred to as a slice of the spectrum of $x(t)$. The ik th element of the $M \times N$ matrix \mathbf{A} is given by

$$\mathbf{A}_{ik} = \frac{1}{NT_{\text{Nyq}}} e^{j\frac{2\pi}{N}c_i K_k}, \quad (21)$$

namely \mathbf{A} is determined by the known sampling pattern $\{c_i\}_{i=1}^M$.

B. MWC sampling

The MWC [13] is composed of M parallel channels. In each channel, an analog mixing front-end, where $x(t)$ is multiplied by a mixing function $p_i(t)$, aliases the spectrum, such that each band appears in baseband. The mixing functions $p_i(t)$ are required to be periodic with period T_p such that $f_p = 1/T_p \geq B$. The function $p_i(t)$ has a Fourier expansion

$$p_i(t) = \sum_{l=-\infty}^{\infty} c_{il} e^{j\frac{2\pi}{T_p} l t}. \quad (22)$$

In each channel, the signal goes through a lowpass filter with cut-off frequency $f_s/2$ and is sampled at the rate $f_s \geq f_p$, resulting in the samples $y_i[n]$. For the sake of simplicity, we choose $f_s = f_p$. Define

$$N = \left\lceil \frac{f_{\text{Nyq}}}{f_s} \right\rceil. \quad (23)$$

Repeating the calculations in [13], we derive the relation between the known DTFTs of the samples $y_i[n]$ and the unknown $X(f)$

$$\mathbf{z}(\tilde{f}) = \mathbf{A}\mathbf{x}(\tilde{f}), \quad \tilde{f} \in \mathcal{F}_s, \quad (24)$$

where $\mathbf{z}(\tilde{f})$ is a vector of length N with i th element $z_i(\tilde{f}) = Y_i(e^{j2\pi\tilde{f}T_s})$. The unknown vector $\mathbf{x}(\tilde{f})$ is given by (20). The $M \times N$ matrix \mathbf{A} contains the known coefficients c_{il} such that

$$\mathbf{A}_{il} = c_{i,-l} = c_{il}^*. \quad (25)$$

Systems (19) and (24) are identical for both sampling schemes: the only difference is the sampling matrix \mathbf{A} . In the next section, we derive a method for reconstruction of the analog cyclic spectrum for both sampling schemes jointly. In particular, we will reconstruct $S_x^\alpha(f)$ from correlations between shifted versions of $\mathbf{z}(\tilde{f})$, defined in (19) and (24). We note that for both sampling schemes, the overall sampling rate is

$$f_{\text{tot}} = Mf_s = \frac{M}{N} f_{\text{Nyq}}. \quad (26)$$

IV. CYCLIC SPECTRUM RECONSTRUCTION

In this section, we provide a method to reconstruct the cyclic spectrum $S_x^\alpha(f)$ of $x(t)$ from sub-Nyquist samples obtained using either of the sampling schemes described above, namely multicoset and the MWC. We also investigate the cyclic spectrum recovery conditions, that is the minimal sampling rate allowing for perfect recovery of $S_x^\alpha(f)$ in the presence of stationary noise. Finally, we evoke the special case of power spectrum reconstruction, presented in [18], and compare it to cyclic spectrum both in terms of recovery method and conditions.

A. Relation between Samples and Cyclic Spectrum

From (19) or (24), we have

$$\mathbf{R}_z^a(\tilde{f}) = \mathbf{A}\mathbf{R}_x^a(\tilde{f})\mathbf{A}^H, \quad \tilde{f} \in [0, f_s - a], \quad (27)$$

for all $a \in [0, f_s]$, where

$$\mathbf{R}_x^a(\tilde{f}) = \mathbb{E} \left[\mathbf{x}(\tilde{f})\mathbf{x}^H(\tilde{f} + a) \right], \quad (28)$$

and

$$\mathbf{R}_z^a(\tilde{f}) = \mathbb{E} \left[\mathbf{z}(\tilde{f})\mathbf{z}^H(\tilde{f} + a) \right]. \quad (29)$$

Here $(\cdot)^H$ denotes the Hermitian operation. The entries in the matrix $\mathbf{R}_x^a(\tilde{f})$ are correlations between shifted versions of the slices $\mathbf{x}(f)$, namely correlations between frequency-shifted versions of $x(t)$. The variable a controls the shift between the slices, while \tilde{f} , running in the interval $[0, f_s - a]$, determines the specific frequency location within the slice. Both a and \tilde{f} are continuous and $\mathbf{R}_x^a(\tilde{f})$ can be computed for any combination of $a \in [0, f_s]$ and $\tilde{f} \in [0, f_s - a]$. In practice, with a limited sensing time, a and \tilde{f} are discretized according to the number of samples per channel.

To proceed, we begin by investigating the link between the cyclic spectrum $S_x^\alpha(f)$ and the shifted correlations between the slices $\mathbf{x}(\tilde{f})$, namely the entries of $\mathbf{R}_x^a(\tilde{f})$. We then show how the latter can be recovered from $\mathbf{R}_z^a(\tilde{f})$ using (27).

The alternative definition of the cyclic spectrum (10) implies that the elements in the matrix $\mathbf{R}_x^a(\tilde{f})$ are equal to $S_x^\alpha(f)$ at the corresponding α and f . Indeed, it can easily be shown that

$$\mathbf{R}_x^a(\tilde{f})_{(i,j)} = S_x^\alpha(f), \quad (30)$$

for

$$\begin{aligned} \alpha &= (j-i)f_s + a \\ f &= -\frac{f_{\text{Nyq}}}{2} + \tilde{f} - \frac{f_s}{2} + \frac{(j+i)f_s}{2} + \frac{a}{2}. \end{aligned} \quad (31)$$

Here $\mathbf{R}_x^a(\tilde{f})_{(i,j)}$ denotes the (i,j) th element of $\mathbf{R}_x^a(\tilde{f})$. In particular, from (15), it follows that for $a = 0$, namely with no shift, it holds that

$$\mathbf{R}_x^0(\tilde{f}) = \sum_{k=1}^{N_{\text{sig}}} \mathbf{R}_{s_k}^0(\tilde{f}) + \mathbf{R}_n^0(\tilde{f}). \quad (32)$$

Here, $\mathbf{R}_n^0(\tilde{f})$ is a diagonal matrix that contains the noise's power spectrum, such that

$$\mathbf{R}_n^0(\tilde{f})_{kk} = S_n^0 \left(-\frac{f_{\text{Nyq}}}{2} + kf_s + \tilde{f} \right), \quad (33)$$

for $0 \leq k \leq N-1$, and

$$\mathbf{R}_{\mathbf{s}_k}^a(\tilde{f}) = \mathbb{E} \left[\mathbf{s}_k(\tilde{f}) \mathbf{s}_k^H(\tilde{f} + a) \right], \quad (34)$$

where $\mathbf{s}_k(\tilde{f})$ is a vector of size N whose non zero elements are the frequency slices from $\mathbf{x}(\tilde{f})$ corresponding to the k th transmission. The diagonal of $\mathbf{R}_{\mathbf{x}}^0(\tilde{f})_{kk}$ contains the power spectrum of $x(t)$ such that

$$\mathbf{R}_{\mathbf{x}}^0(\tilde{f})_{kk} = S_x^0 \left(-\frac{f_{\text{Nyq}}}{2} + kf_s + \tilde{f} \right), \quad (35)$$

for $0 \leq k \leq N-1$, is the sum of the transmissions' and noise's power spectrum. Since $n(t)$ is stationary, for $a \neq 0$, we have

$$\mathbf{R}_{\mathbf{x}}^a(\tilde{f}) = \sum_{k=1}^{N_{\text{sig}}} \mathbf{R}_{\mathbf{s}_k}^a(\tilde{f}). \quad (36)$$

Our goal can then be stated as recovery of $\mathbf{R}_{\mathbf{x}}^a(\tilde{f})$, for $a \in [0, f_s]$ and $\tilde{f} \in [0, f_s - a]$, since once $\mathbf{R}_{\mathbf{x}}^a(\tilde{f})$ is known, $S_x^\alpha(f)$ follows for all (α, f) , using (30).

We now consider the structure of the autocorrelation matrices $\mathbf{R}_{\mathbf{x}}^a(\tilde{f})$, which is related to the support of the cyclic spectrum $S_x^\alpha(f)$. In Section II-B, we discussed the support of $S_x^\alpha(f)$, composed of two types of correlations: self-correlations between a band and its shifted version and cross-correlations between shifted versions of symmetric bands belonging to the same transmission. Consider a given frequency location \tilde{f} and shift a . The frequency component $\mathbf{x}_i(\tilde{f})$, for $0 \leq i \leq N-1$, with N defined in (23), can be correlated to at most two entries of $\mathbf{x}(\tilde{f} + a)$, one from the same band and one from the symmetric band. The correlated component can be either in the same - symmetric - slice or in one of the adjacent slices. This follows from the fact that each band can split between two slices at most, since we require $f_p \geq B$. Thus, the first correlated entry is either i or $i \pm 1$ and the second is either $N-i$, $N-i+1$ or $N-1+2$. Note that since the noise is assumed to be wide-sense stationary, from (11), a noise frequency component is correlated only with itself. Thus, $n(t)$ only contributes non-zero elements on the diagonal of $\mathbf{R}_{\mathbf{x}}^0(\tilde{f})$.

Figures 3 and 4 illustrate these correlations for $a = 0$ and $a = f_s/2$, respectively. First, in Fig. 2, an illustration of the spectrum of $x(t)$, namely $X(f)$, is presented for the case of a sparse signal buried in stationary bandpass noise. It can be seen that frequency bands of $X(f)$ can either appear in one f_p -slice or split between two slices. The resulting vector of spectrum slices $\mathbf{x}(f)$ and the correlations between these slices without any shift, namely $\mathbf{R}_{\mathbf{x}}^0(\tilde{f})$, are shown in Fig. 3(a) and (b), respectively. Define the d -diagonal and d -anti diagonal of an $N \times N$ matrix to be its (i, j) th elements such that $j = i + d$, and $j = N - i + 1 - d$, respectively. In particular, the 0-diagonal stands for the main diagonal and the 0-anti diagonal is the secondary diagonal. In Fig. 3(b), we



Fig. 2. Original spectrum $X(f)$.

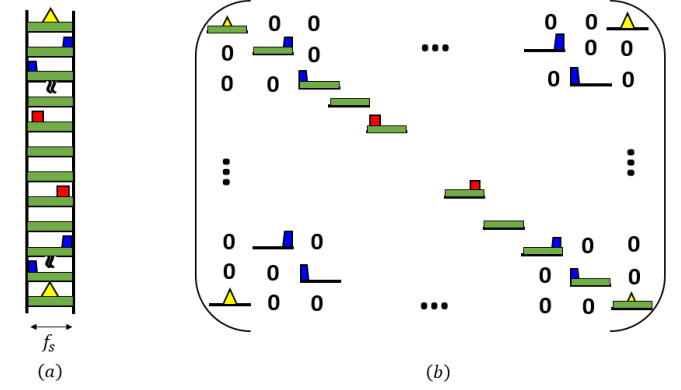


Fig. 3. (a) Spectrum slices vector $\mathbf{x}(\tilde{f})$, (b) correlated slices of $\mathbf{x}(\tilde{f})$ in the matrix $\mathbf{R}_{\mathbf{x}}^0(\tilde{f})$.

observe that self-correlations appear only on the main diagonal since every frequency component is correlated with itself. In particular, the main diagonal contains the noise's power spectrum (in green). Cross-correlations between the yellow symmetric triangles appear in the 0-anti diagonal, whereas those of the blue trapezoids are contained in the -1 and 1 -anti diagonals. The red rectangles do not contribute any cross-correlations for a shift of $a = 0$. Figures 4(a) and (b) show the vector $x(\tilde{f})$ and its shifted version $x(\tilde{f} + a)$ for $a = f_s/2$, respectively. The resulting correlation matrix $\mathbf{R}_{\mathbf{x}}^a(\tilde{f})$ appears in Figure 4(c). Here, the self correlations of the yellow triangle appear in the main diagonal and that of the blue trapezoid in the -1 -diagonal. The cross-correlations all appear in the anti-diagonal, for the shift $a = f_s/2$.

The following four conclusions can be drawn from the observation above on the structure of $\mathbf{R}_{\mathbf{x}}^a(\tilde{f})$, for a given $a \in]0, f_s]$ and $\tilde{f} \in [0, f_s - a]$. We will treat the case where $a = 0$ separately since it yields a different structure due to the presence of noise.

- **Conclusion 1:** The non zero entries of $\mathbf{R}_{\mathbf{x}}^a(\tilde{f})$ are contained in its -1 , 0 and 1 -diagonals and -1 , 0 and 1 -anti diagonals.
- **Conclusion 2:** The i th row of $\mathbf{R}_{\mathbf{x}}^a(\tilde{f})$ contains at most two non zero elements at locations $(i, g(i))$ and $(i, g(N - i + 1))$, where

$$g(i) = \begin{cases} i \text{ or } i \pm 1 & 2 \leq i \leq N - 1, \\ i \text{ or } i + 1 & i = 1, \\ i \text{ or } i - 1 & i = N. \end{cases} \quad (37)$$

- **Conclusion 3:** The j th column of $\mathbf{R}_{\mathbf{x}}^a(\tilde{f})$ contains at most two non zero elements at locations $(g(j), j)$ and

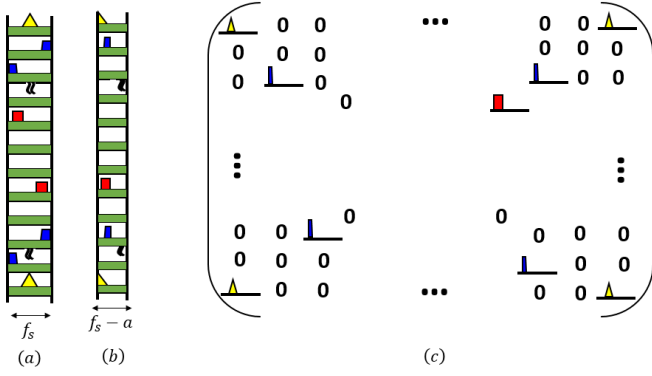


Fig. 4. (a) Spectrum slices vector $\mathbf{x}(\tilde{f})$ (b) spectrum slices shifted vector $\mathbf{x}(\tilde{f} + a)$, for $a = f_s/2$, (c) correlated slices of $\mathbf{x}(\tilde{f})$ and $\mathbf{x}(\tilde{f} + a)$ in the matrix $\mathbf{R}_x^a(\tilde{f})$, with $a = f_s/2$.

$(g(N - j + 1), j)$, for $1 \leq j \leq N$.

- **Conclusion 4:** For each specific frequency \tilde{f} , a transmission contributes to at most two slices, one in the negative and one in the positive frequencies. This is due to the assumption that $f_p \geq B$. Therefore, $\mathbf{R}_x^a(\tilde{f})$ contains at most $K = 2N_{\text{sig}}$ rows/columns that have non zero elements. Without any sparsity assumption, it is obvious that $K = N$ even if the number of transmissions is greater than $N/2$.

From **Conclusions 2** and **4**, it follows that $\mathbf{R}_x^a(\tilde{f})$ is $2K$ -sparse and has additional structure described in **Conclusions 1-3**.

Since the non zero elements of $\mathbf{R}_x^a(\tilde{f})$ only lie on the 3 main and anti-diagonals, (27) can be further reduced to

$$\mathbf{r}_z^a(\tilde{f}) = (\bar{\mathbf{A}} \otimes \mathbf{A}) \text{vec}(\mathbf{R}_x^a(\tilde{f})) = (\bar{\mathbf{A}} \otimes \mathbf{A}) \mathbf{B} \mathbf{r}_x^a(\tilde{f}) \triangleq \Phi \mathbf{r}_x^a(\tilde{f}), \quad (38)$$

where $\bar{\mathbf{A}}$ denotes the conjugate matrix of \mathbf{A} and

$$\Phi = (\bar{\mathbf{A}} \otimes \mathbf{A}) \mathbf{B}. \quad (39)$$

Here \otimes is the Kronecker product, $\mathbf{r}_z^a(\tilde{f}) = \text{vec}(\mathbf{R}_z^a(\tilde{f}))$, where $\text{vec}(\cdot)$ denotes the column stack concatenation operation, and \mathbf{B} is a $N^2 \times (6N - 4)$ selection matrix that selects the elements of the $-1, 0$ and 1 -diagonals and anti-diagonals of $\mathbf{R}_x^a(\tilde{f})$ from the vector $\text{vec}(\mathbf{R}_x^a(\tilde{f}))$. The resulting $(6N - 4) \times 1$ vector composed of these selected elements is denoted by $\mathbf{r}_x^a(\tilde{f})$.

From **Conclusions 2-4**, the vector $\mathbf{r}_x^a(\tilde{f})$ is $2K$ -sparse and its support presents additional structure. Denote by Σ_k the set of k -sparse vectors that belong to a linear subspace Σ . In our case, $\mathbf{r}_x^a(\tilde{f})$ belongs to $\Sigma_k = \Sigma_{2K}$, defined as

$$\Sigma_{2K} = \{\mathbf{x} \in \mathbb{R}^{(6N-4) \times 1} \mid |S(\mathbf{x})| \leq 2K \wedge S(\mathbf{x}) \in \mathcal{I}\}, \quad (40)$$

where $S(\mathbf{x})$ denotes the support of \mathbf{x} and the set \mathcal{I} is determined by the following properties:

- 1) If the group indexed by j is in \mathcal{I} , then the group indexed by $(N + 1 - j)$ is in \mathcal{I} as well. The groups are defined in the following items.
- 2) If the group indexed by $2 \leq j \leq N - 1$ is in \mathcal{I} , then it means that at most one of the entries $\{6j - 1, 6j, 6j + 1\}$

and at most one of the entries $\{6j + 2, 6j + 3, 6j + 4\}$ are in \mathcal{I} .

- 3) If the group indexed by $j = 1$, then at most one of the entries $\{1, 2\}$ and at most one of the entries $\{3, 4\}$ are in \mathcal{I} .
- 4) If the group indexed by $j = N$, then at most one of the entries $\{6N - 7, 6N - 6\}$ and at most one of the entries $\{6N - 5, 6N - 4\}$ are in \mathcal{I} .

Item 1) follows from **Conclusion 4** and items 2)-3) and 4) follow from **Conclusions 2-3**. We note that the indexation above is valid if the selection matrix in (38) selects the elements of $\text{vec}(\mathbf{R}_x^a(\tilde{f}))$ row by row. Any other selection order would yield a different indexation.

Consider now the case where $a = 0$. The matrix $\mathbf{R}_x^0(\tilde{f})$ contains the power spectrum of the transmissions and the noise on its main diagonal and cyclic components of the transmissions on its $-1, 0$ and 1 -anti diagonals. The remaining elements are zero. Denote by $\mathbf{r}_{x_1}^0$ the $N \times 1$ non-sparse vector composed of the diagonal of $\mathbf{R}_x^0(\tilde{f})$ and by $\mathbf{r}_{x_2}^0$ the $(3N - 2) \times 1$ sparse vector composed of its $-1, 0$ and 1 -anti diagonals. Let $\Phi_1 = \bar{\mathbf{A}} \odot \mathbf{A}$ where \odot denotes the Khatri-Rao product and $\Phi_2 = (\bar{\mathbf{A}} \otimes \mathbf{A}) \bar{\mathbf{B}}$ with $\bar{\mathbf{B}}$ a $N^2 \times (3N - 2)$ selection matrix that selects the elements of the $-1, 0$ and 1 -anti diagonals of $\mathbf{R}_x^0(\tilde{f})$ from the vector $\text{vec}(\mathbf{R}_x^0(\tilde{f}))$. Combining (32) and (38), we can write $\mathbf{r}_z^0(\tilde{f})$ as the sum of two components as follows,

$$\mathbf{r}_z^0(\tilde{f}) = \Phi_2 \mathbf{r}_{x_2}^0(\tilde{f}) + \mathbf{w}(\tilde{f}), \quad (41)$$

where $\mathbf{w}(\tilde{f}) = \Phi_1 \mathbf{r}_{x_1}^0(\tilde{f})$ is the noise component. We note that the signal's power spectrum is buried in the noise $\mathbf{w}(\tilde{f})$. Therefore, we do not recover it and signal detection will be performed only on cyclic frequencies $\alpha \neq 0$.

From (14) and (30), by recovering $\mathbf{r}_x^a(\tilde{f}) \in \Sigma_{2K}$ for all $a \in [0, f_s]$, $\tilde{f} \in [0, f_s - a]$, we recover the entire cyclic spectrum of $x(t)$. We consider only $a \geq 0$ and consequently $\alpha \geq 0$. We thus only reconstruct half of the cyclic spectrum, known to be symmetric [6]. In (38), there is no noise component, even if the signal $x(t)$ is corrupted by additional stationary noise. For the corresponding cyclic frequencies, we can therefore achieve recovery. In contrast, in (41), namely for $a = 0$, there is an additional noise component. From (31), this case corresponds to cyclic frequencies which are multiple of the channels' sampling frequency f_s . In this case, the recovery of the sparse vector $\mathbf{r}_{x_2}^0(\tilde{f}) \in \Sigma_{2K}$ is not perfect and is performed in the presence of bounded noise. In the simulations, we observe that for detection purposes, this noisy recovery is satisfactory. To achieve perfect recovery for these cyclic frequencies as well, we can sample the signal with the exact same sampling scheme (multicoreset or MWC) using a different sampling frequency f_{s_2} . However, this increases the overall sampling rate by a factor of 2.

B. Cyclic Spectrum Recovery Conditions

We now consider conditions for perfect recovery of the cyclic spectrum $S_x^\alpha(f)$ from the sub-Nyquist samples. Theorem 2 below derives sufficient conditions on the minimal number of channels M for perfect recovery of $\mathbf{R}_x^a(\tilde{f})$, for

any $a \in [0, f_s]$ and $\tilde{f} \in [0, f_s - a]$ in the presence of additive stationary noise. As stated above, for $a = 0$, the recovery is noisy. From **Conclusion 1**, we only need to recover $\mathbf{r}_x^a(\tilde{f})$ from (38) or (41) for $a \neq 0$ or $a = 0$, respectively. Theorem 1 first states sufficient conditions for the reconstruction of the vector $\mathbf{r}_x^a(\tilde{f}) \in \Sigma_{2K}$. To that end, we rely on the following Lemma which is well known in the CS literature [15], [31].

Lemma 1. *For any vector $\mathbf{y} \in \mathbb{R}^m$, there exists at most one signal $\mathbf{x} \in \Sigma_k$ such that $\mathbf{y} = \mathbf{A}\mathbf{x}$ if and only if all sets of $2k$ columns of \mathbf{A} belonging to W , such that*

$$W = \{S(\mathbf{x}_1) \cup S(\mathbf{x}_2) | \mathbf{x}_1, \mathbf{x}_2 \in \Sigma_k\}, \quad (42)$$

are linearly independent. In particular, for uniqueness we must have that $m \geq 2k$.

Using Lemma 1, it follows that in order to perfectly recover $\mathbf{r}_x^a(\tilde{f}) \in \Sigma_{2K}$ from $\mathbf{r}_z^a(\tilde{f})$, we need to ensure that all sets of $4K$ columns of Φ belonging to W are linearly independent. In our case, W is the set of unions of the supports of two vectors from Σ_{2K} , as defined in (42). The following theorem relates spark properties of the sampling matrix \mathbf{A} to rank properties of sub-matrices of Φ of size $M^2 \times 4K$, whose columns belong to W , which we denote by Φ^W . Since Φ_2 in (41) is a submatrix of Φ , we only need to consider recovery conditions for the case $a \neq 0$. For $a = 0$, under these conditions, we do not achieve perfect recovery due to the presence of the noise component in (41).

Theorem 1. *Let Φ be defined in (39), with \mathbf{A} full spark of size $M \times N$ ($M \leq N$). The $M^2 \times 4K$ matrix Φ^W , whose columns belong to W defined in (42) with $\Sigma_k = \Sigma_{2K}$ from (40), is full column rank if $M > \frac{8}{5}K$.*

We note that if $K \geq 2$, namely there is at least one transmission, then $M > \frac{8}{5}K$ implies $M^2 \geq 4K$ and Φ^W is a tall matrix.

Proof: Recall that the matrix Φ is expressed as

$$\begin{aligned} \Phi = & [\bar{\mathbf{a}}_1 \otimes \mathbf{a}_1 \quad \bar{\mathbf{a}}_2 \otimes \mathbf{a}_2 \quad \dots \quad \bar{\mathbf{a}}_N \otimes \mathbf{a}_N \quad \dots \\ & \dots \quad \bar{\mathbf{a}}_1 \otimes \mathbf{a}_2 \quad \bar{\mathbf{a}}_2 \otimes \mathbf{a}_3 \quad \dots \quad \bar{\mathbf{a}}_{N-1} \otimes \mathbf{a}_N \\ & \dots \quad \bar{\mathbf{a}}_2 \otimes \mathbf{a}_1 \quad \bar{\mathbf{a}}_3 \otimes \mathbf{a}_2 \quad \dots \quad \bar{\mathbf{a}}_N \otimes \mathbf{a}_{N-1} \\ & \bar{\mathbf{a}}_1 \otimes \mathbf{a}_N \quad \bar{\mathbf{a}}_2 \otimes \mathbf{a}_{N-1} \quad \dots \quad \bar{\mathbf{a}}_N \otimes \mathbf{a}_1 \quad \dots \\ & \dots \quad \bar{\mathbf{a}}_1 \otimes \mathbf{a}_{N-1} \quad \bar{\mathbf{a}}_2 \otimes \mathbf{a}_{N-2} \quad \dots \quad \bar{\mathbf{a}}_{N-1} \otimes \mathbf{a}_1 \\ & \dots \quad \bar{\mathbf{a}}_2 \otimes \mathbf{a}_N \quad \bar{\mathbf{a}}_3 \otimes \mathbf{a}_{N-1} \quad \dots \quad \bar{\mathbf{a}}_N \otimes \mathbf{a}_2 \quad]. \end{aligned} \quad (43)$$

Assume by contradiction that the columns of Φ^W are linearly dependent. Then, there exists $\beta_1, \dots, \beta_{4K}$, not all zeros, such that

$$\sum_{j=1}^{4K} \beta_j \phi_j^W = \mathbf{0}, \quad (44)$$

where ϕ_j^W denotes the j th column of Φ^W and is of the form

$$\phi_j^W = \bar{\mathbf{a}}_{[j]} \otimes \mathbf{a}_{g([j])} \text{ or } \bar{\mathbf{a}}_{[j]} \otimes \mathbf{a}_{g([N+1-j])}. \quad (45)$$

Here $\mathbf{a}_{[j]}$ denotes the column of \mathbf{A} that corresponds to the j th selected column of Φ and $g(\cdot)$ is defined in (37). Denote by

k_0 the number of indices $[j]$, for $1 \leq j \leq K$, that appear twice in Φ^W . Obviously, $0 \leq k_0 \leq K$ and k_0 is even.

From 1)-4) in the definition of Σ_{2K} , we can express Φ^W as

$$\begin{aligned} \Phi^W = & [\bar{\mathbf{a}}_{[1]} \otimes \mathbf{a}_{g([1])} \quad \dots \quad \bar{\mathbf{a}}_{[K]} \otimes \mathbf{a}_{g([K])} \quad \dots \\ & \dots \quad \bar{\mathbf{a}}_{[1]} \otimes \mathbf{a}_{h([1])} \quad \dots \quad \bar{\mathbf{a}}_{[k_0/2]} \otimes \mathbf{a}_{h([k_0/2])} \quad \dots \\ & \dots \quad \bar{\mathbf{a}}_{[K-k_0/2]} \otimes \mathbf{a}_{h([K-k_0/2])} \quad \dots \quad \bar{\mathbf{a}}_{[K]} \otimes \mathbf{a}_{h([K])} \quad \dots \\ & \dots \quad \bar{\mathbf{a}}_{[K+1]} \otimes \mathbf{a}_{g([K+1])} \quad \dots \quad \bar{\mathbf{a}}_{[2K-k_0]} \otimes \mathbf{a}_{g([2K-k_0])} \quad \dots \\ & \dots \quad \bar{\mathbf{a}}_{[1]} \otimes \mathbf{a}_{g([K])} \quad \dots \quad \bar{\mathbf{a}}_{[K]} \otimes \mathbf{a}_{g([1])} \quad \dots \\ & \dots \quad \bar{\mathbf{a}}_{[1]} \otimes \mathbf{a}_{h([K])} \quad \dots \quad \bar{\mathbf{a}}_{[k_0/2]} \otimes \mathbf{a}_{h([K-k_0/2])} \quad \dots \\ & \dots \quad \bar{\mathbf{a}}_{[k_0/2]} \otimes \mathbf{a}_{h([K-k_0/2])} \quad \dots \quad \bar{\mathbf{a}}_{[K]} \otimes \mathbf{a}_{h([1])} \quad \dots \\ & \dots \quad \bar{\mathbf{a}}_{[K+1]} \otimes \mathbf{a}_{g([2K-k_0])} \quad \dots \quad \bar{\mathbf{a}}_{g([2K-k_0])} \otimes \mathbf{a}_{g([K+1])}]. \end{aligned} \quad (46)$$

Here, $h(i)$ is defined as $g(i)$ and we can have either $h(i) = g(i)$ or $h(i) \neq g(i)$. It can then easily be shown that the system of equations (44) can be rearranged as follows

$$\mathbf{C}\bar{\mathbf{A}}^T = \mathbf{0}, \quad (47)$$

where the $M \times (2K - k_0)$ matrix \mathbf{C} is defined as

$$\begin{aligned} \mathbf{C} = & [\beta_1 \mathbf{a}_{g([1])} + \beta_{K+1} \mathbf{a}_{h([1])} + \beta_{2K+1} \mathbf{a}_{g([K])} + \beta_{3K+1} \mathbf{a}_{h([K])} \\ & \dots \quad \beta_K \mathbf{a}_{g([K])} + \beta_{K+k_0} \mathbf{a}_{h([K])} + \beta_{3K} \mathbf{a}_{g([1])} + \beta_{3K+k_0} \mathbf{a}_{h([1])} \\ & \dots \quad \beta_{K+k_0+1} \mathbf{a}_{g([K+1])} + \beta_{3K+k_0+1} \mathbf{a}_{g([2K-k_0])} \\ & \dots \quad \beta_{2K} \mathbf{a}_{g([2K-k_0])} + \beta_{4K} \mathbf{a}_{g([K+1])}]. \end{aligned} \quad (48)$$

Denote by n_0 the number of quadruplets $(\beta_j, \beta_{K+j}, \beta_{2K+j}, \beta_{3K+j})$, for $1 \leq j \leq K$, or pairs $(\beta_{k_0+j}, \beta_{2K+k_0+j})$, for $K+1 \leq j \leq 2K - k_0$, with one non zero element at least. Obviously $1 \leq n_0 \leq 2K - k_0$. Let $\tilde{\mathbf{C}}$ be the $M \times n_0$ matrix composed of the n_0 columns of \mathbf{C} corresponding to these non zero quadruplets/pairs and let $\tilde{\mathbf{A}}^T$ be constructed out of the corresponding n_0 rows of $\bar{\mathbf{A}}^T$. Then, from the Sylvester rank inequality,

$$\text{rank}(\mathbf{C}\bar{\mathbf{A}}^T) = \text{rank}(\tilde{\mathbf{C}}\tilde{\mathbf{A}}^T) \geq \text{rank}(\tilde{\mathbf{C}}) + \text{rank}(\tilde{\mathbf{A}}^T) - n_0. \quad (49)$$

In addition,

$$\text{rank}(\tilde{\mathbf{A}}^T) \geq \min(n_0, \text{spark}(\mathbf{A}) - 1), \quad (50)$$

and

$$\text{rank}(\tilde{\mathbf{C}}) \geq \min\left(\left\lceil \frac{n_0}{4} \right\rceil, \frac{\text{spark}(\mathbf{A}) - 1}{4}\right). \quad (51)$$

The last inequality follows from the fact that any linear combination of n columns of \mathbf{C} is a linear combination of at least $\lceil n/4 \rceil$ distinct columns of \mathbf{A} . Therefore,

$$\text{rank}(\mathbf{C}\bar{\mathbf{A}}^T) \geq \min\left(\left\lceil \frac{n_0}{4} \right\rceil, \frac{5}{4}M - n_0\right). \quad (52)$$

Since $M > \frac{8}{5}K$, it holds that $\text{rank}(\mathbf{C}\bar{\mathbf{A}}^T) \geq 1$, for all $1 \leq n_0 \leq 2K - k_0$, $0 \leq k_0 \leq K$, leading to a contradiction with (47). \square

The following theorem provides sufficient conditions for perfect recovery of $\mathbf{r}_x^a(\tilde{f})$.

Theorem 2. *If*

- 1) \mathbf{A} is full spark,
- 2) $M > \frac{8}{5}K$,

then the system (38) has a unique solution in Σ_{2K} .

Proof: Conditions 1)-2) ensure that all sets of $2K$ columns belonging to W are linearly independent, from Proposition 1. Thus, the proof follows from Theorem 1. \square

Under the conditions of Theorem 2, the cyclic spectrum $S_x(f)$ can be perfectly recovered for cyclic frequencies α which are not multiples of f_s . For α that are multiples of f_s , the recovery is performed in the presence of bounded noise, yielding a bounded reconstruction error. For detection purposes, this has proven satisfactory in the simulations.

Without any sparsity assumption, we can repeat the proof of Proposition 1 with $K = N$ and $k_0 = N$, leading to $1 \leq n_0 \leq N$. We thus obtain that, if $M > \frac{4}{5}N$, then we can perfectly recover the cyclic spectrum of $x(t)$. The minimal sampling rate is then

$$f_{\min_0} = Mf_s = \frac{4}{5}Nf_s = \frac{4}{5}f_{\text{Nyq}}. \quad (53)$$

This means that even without any sparsity constraints on the signal, we can retrieve its cyclic spectrum from samples below the Nyquist rate, by exploiting its cyclostationary properties. A similar result was already observed in [18] in the context of power spectrum reconstruction of wide-sense stationary signals in noiseless settings. In that case, the power spectrum slices appear only on the diagonal of the matrix $\mathbf{R}_x^0(f)$ and it follows that $\Phi = \bar{\mathbf{A}} \odot \mathbf{A}$. Power spectrum recovery is therefore a special case of cyclic spectrum reconstruction, treated here. There, it was shown that the power spectrum can be retrieved at half the Nyquist rate without any sparsity constraints. Here, we extend this result to cyclic spectrum reconstruction, which requires a higher rate.

If $x(t)$ is assumed to be sparse in the frequency domain, with $K = 2N_{\text{sig}} \ll N$, then the minimal sampling rate for perfect reconstruction of its cyclic spectrum is

$$f_{\min} = Mf_s = \frac{16}{5}N_{\text{sig}}B = \frac{8}{5}f_{\text{Landau}}. \quad (54)$$

It was shown in [18], that the power spectrum of a stationary sparse signal can be perfectly recovered at its Landau rate. Again, the minimal sampling rate for cyclic spectrum recovery is slightly higher than the rate required for power spectrum reconstruction.

C. Cyclic Spectrum Recovery

So far, we only discussed the conditions for perfect recovery of the cyclic spectrum, namely for (38) and (41) to have unique solutions. We now turn to the actual cyclic spectrum's reconstruction and provide a concrete algorithm for it. The cyclic spectrum reconstruction of both sparse and non sparse signals can be divided into two stages: support recovery and cyclic spectrum recovery. We use the support recovery paradigm from [12] that produces a finite system of equations, called multiple measurement vectors (MMV) from an infinite number of linear systems. This reduction is performed by what

is referred to as the continuous to finite (CTF) block. From (38), for $a \in]0, f_s]$, we have

$$\mathbf{Q}^a = \Phi \mathbf{Z}^a \Phi^H \quad (55)$$

where

$$\mathbf{Q}^a = \int_{\tilde{f} \in \mathcal{F}_s} \mathbf{r}_z^a(\tilde{f}) \mathbf{r}_z^{aH}(\tilde{f}) d\tilde{f} \quad (56)$$

is an $M \times M$ matrix and

$$\mathbf{Z}^a = \int_{\tilde{f} \in \mathcal{F}_s} \mathbf{r}_x^a(\tilde{f}) \mathbf{r}_x^{aH}(\tilde{f}) d\tilde{f} \quad (57)$$

is an $N \times N$ matrix. We then construct a frame \mathbf{V}^a such that $\mathbf{Q}^a = \mathbf{V}^a (\mathbf{V}^a)^H$. Clearly, there are many possible ways to select \mathbf{V} . We construct it by performing an eigendecomposition of \mathbf{Q}^a and choosing \mathbf{V}^a as the matrix of eigenvectors corresponding to the non zero eigenvalues. We can then define the following linear system

$$\mathbf{V}^a = \Phi \mathbf{U}^a. \quad (58)$$

For $a = 0$, identical derivations can be carried out by replacing Φ by Φ_2 . From [12] (Propositions 2-3), the support of the unique sparsest solution of (58) is the same as the support of $\mathbf{r}_x^a(f)$ in our original set of equations (38) (or (41)).

As discussed above, $\mathbf{r}_x^a(\tilde{f})$ is $2K$ -sparse for each specific $\tilde{f} \in [0, f_s - a]$, for all $a \in [0, f_s]$. However, after combining the frequencies, the matrix \mathbf{U}^a is $4K$ -sparse (at most), since the spectrum of each transmission can split between two slices. Therefore, the above algorithm, referred to as SBR4 in [12] (for signal reconstruction as opposed to cyclic spectrum reconstruction), requires a minimal sampling rate of $2f_{\min}$ for sparse signals or $2f_{\min_0}$ for non sparse signals. In order to achieve the minimal rate f_{\min} or f_{\min_0} , the SBR2 algorithm regains the factor of two in the sampling rate at the expense of increased complexity [12]. In a nutshell, SBR2 is a recursive algorithm that alternates between the CTF described above and a bi-section process. The bi-section splits the original frequency interval into two equal width intervals on which the CTF is applied, until the level of sparsity of \mathbf{U}^a is less or equal to $2K$. We refer the reader to [12] for more details.

For the CTF stage, we extend the orthogonal matching pursuit (OMP) [15], [31] to account for the structure of $\mathbf{r}_x^a(f)$ for $a \neq 0$. In each iteration, we add an internal loop that, for a selected element originally from the diagonals of $\mathbf{R}_x^a(f)$, checks for a corresponding non-zero element from the anti-diagonals, and vice versa, as defined by the set \mathcal{I} . For $a = 0$, we use the standard OMP [15], [31]. We note that for all $a \geq 0$ we can exploit the additional symmetric structure $\mathbf{r}_x^a(f)$ as defined by Property 1 of \mathcal{I} . However, this would further increase the algorithm complexity. Our structured OMP method (assuming that the columns of Φ are normalized) is formally defined by Algorithm 1. For simplicity, we present the SMV (single measurement vector) version, which can be adapted to the MMV settings similarly to the simultaneous OMP [15], [31].

Algorithm 1 Structured Orthogonal Matching Pursuit

Input: observation vector \mathbf{v} of size m , measurement matrix Φ of size $m \times n$, threshold $\epsilon > 0$
Output: index set S containing the locations of the non zero indices of \mathbf{u} , estimate for sparse vector $\hat{\mathbf{u}}$
Initialize: residual $\mathbf{r}_0 = \mathbf{v}$, index set $S_0 = \emptyset$, possible index set $\Gamma_0 = \{1, \dots, n\}$, estimate $\hat{\mathbf{u}} = \mathbf{0}$, $\ell = 0$
while halting criterion false **do**
 $\ell \leftarrow \ell + 1$
 $\mathbf{b} \leftarrow \Phi^* \mathbf{r}_\ell$
 $S_\ell \leftarrow S_\ell \cup \arg \max_{i \in \Gamma_\ell} \mathbf{b}_i$
 $\Gamma_\ell \leftarrow \Gamma_\ell \setminus \Lambda_i$
 $(\hat{\mathbf{u}}_\ell)^{S_\ell} \leftarrow \Phi_{S_\ell}^\dagger \mathbf{v}$, $(\hat{\mathbf{u}}_\ell)^{S_\ell^c} \leftarrow \mathbf{0}$
 $\delta_0 \leftarrow \|\mathbf{v} - \Phi \hat{\mathbf{u}}_\ell\|^2$
 for $j \in \Lambda_i$ **do**
 $\mathbf{w}_j^{S_\ell} \leftarrow \Phi_{S_\ell \cup j}^\dagger \mathbf{v}$, $\mathbf{w}_j^{S_\ell^c} \leftarrow \mathbf{0}$
 $\delta_j \leftarrow \|\mathbf{v} - \Phi \mathbf{w}_j\|^2$
 end for
 if $\delta_0 - \min_{j \in \Lambda_i} \delta_j > \epsilon$ **then**
 $S_\ell \leftarrow S_\ell \cup \arg \min_{j \in \Lambda_i} \delta_j$
 $(\hat{\mathbf{u}}_\ell)^{S_\ell} \leftarrow \Phi_{S_\ell}^\dagger \mathbf{v}$, $(\hat{\mathbf{u}}_\ell)^{S_\ell^c} \leftarrow \mathbf{0}$
 end if
 $\mathbf{r} \leftarrow \mathbf{v} - \Phi \hat{\mathbf{u}}_\ell$
end while
 return S_ℓ and $\hat{\mathbf{u}}_\ell$

In Algorithm 1, Λ_i denotes the set of complementary indices with respect to i according to Property 2 of \mathcal{I} , namely

$$\Lambda_i = \begin{cases} \{6d_i + 5, 6d_i + 6, 6d_i + 7\} & \text{if } 0 < \text{mod}(i - 4, 6) \leq 3 \\ \{6d_i + 8, 6d_i + 9, 6d_i + 10\} & \text{else,} \end{cases} \quad (59)$$

for $2 \leq i \leq N - 1$. Here $d_i = \lfloor \frac{i-4}{6} \rfloor$. For $i = 1$ and $i = N$, Λ_i is similarly defined according to Properties 3 and 4, respectively. The vector \mathbf{w}^S is the reduction of \mathbf{w} to the support S , Φ_S contains the corresponding columns of Φ , S^c denotes the complementary set of S and \dagger is the Moore-Penrose pseudo-inverse. The halting criterion in Algorithm 1, as for standard OMP, can be sparsity-based if the true sparsity is known, or at least an upper bound for it, or residual-based.

Once the support S is known, perfect reconstruction of the cyclic spectrum can be obtained as follows

$$\begin{aligned} (\hat{\mathbf{r}}_{\mathbf{x}}^a)^S(\tilde{f}) &= \Phi_S^\dagger \mathbf{r}_{\mathbf{z}}^a(\tilde{f}) \\ \hat{\mathbf{r}}_{\mathbf{x}_i}^a(\tilde{f}) &= 0 \quad \forall i \notin S, \end{aligned} \quad (60)$$

for all $a \in [0, f_s]$ and

$$\begin{aligned} (\hat{\mathbf{r}}_{\mathbf{x}}^0)^S(\tilde{f}) &= (\Phi_2)_S^\dagger \mathbf{r}_{\mathbf{z}}^0(\tilde{f}) \\ \hat{\mathbf{r}}_{\mathbf{x}_i}^0(\tilde{f}) &= 0 \quad \forall i \notin S. \end{aligned} \quad (61)$$

Then, the cyclic spectrum $S_x^\alpha(f)$ is assembled using (30) for (f, α) defined in (31).

D. Carrier Frequency and Bandwidth Estimation

Once the cyclic spectrum $S_x^\alpha(f)$ is reconstructed from the sub-Nyquist samples, we apply our carrier frequency and bandwidth estimation algorithm from [34]. Our approach is a simple parameter extraction method from the cyclic spectrum of multiband signals. This approach allows the estimation of several carriers and several bandwidths simultaneously, as well as the number of transmissions N_{sig} . The proposed parameter estimation algorithm can be decomposed into the following main five steps: preprocessing, thresholding, clustering, parameter estimation, corrections. Here, we briefly describe the algorithm steps. The reader is referred to [34] for more details.

The preprocessing simply aims at compensating for the presence of stationary noise in the cyclic spectrum at the cyclic frequency $\alpha = 0$, by attenuating the energy of the cyclic spectrum around this frequency. Thresholding is then applied to the resulting cyclic spectrum in order to find its peaks. For each cyclic frequency α , we retain the value of the cyclic spectrum at $f = 0$. The locations and values of the selected peaks are then clustered to find the corresponding cyclic feature. Before separating the clusters, we start by estimating their number using the elbow method, which can be traced to speculation by Thorndike [38]. Clustering is then performed using the k-means method. At the end of the process, each cluster represents a cyclic feature. It follows that, apart from the cluster present in DC which we remove, the number of signals N_{sig} is equal to half the number of clusters. Next, we estimate the carrier frequency f_i and bandwidth B_i of each transmission. The carrier frequency yields the highest correlation [6] and thus the highest peak, at the cyclic frequency equal to twice its value, namely $\alpha = 2f_i$. It is therefore estimated as half the cyclic frequency of the highest peak within the clusters belonging to the same signal. The bandwidth is found by locating the edge of the support of the angular frequencies.

V. SIMULATION RESULTS

We now demonstrate cyclic spectrum reconstruction from sub-Nyquist samples and investigate the performance of our carrier frequency and bandwidth estimation algorithm. We compare the performance of our approach to energy detection. Throughout the simulations we use the MWC analog front-end [33] for the sampling stage.

A. Preliminaries

We begin by explaining how we estimate the elements of $\mathbf{R}_{\mathbf{z}}^a(\tilde{f})$. The overall sensing time is divided into P frames of length Q samples. We first compute the estimates of $\mathbf{z}_i(f)$, $1 \leq i \leq M$, denoted by $\hat{\mathbf{z}}_i(\tilde{f})$, using the fast Fourier transform (FFT) on the samples $\mathbf{z}_i[n]$ over a finite time window. We then estimate the elements of $\mathbf{R}_{\mathbf{z}}^a(\tilde{f})$ as

$$\hat{\mathbf{R}}_{\mathbf{z}}^a(\tilde{f})_{(i,j)} = \frac{1}{P} \sum_{p=1}^P \left(\hat{\mathbf{z}}_i(\tilde{f}) \right)^p \left(\hat{\mathbf{z}}_j(\tilde{f} + a) \right)^p, \quad (62)$$

for $a \in [0, f_s]$ and $f \in [0, f_s - a]$. Here, P is the number of frames for the averaging of the spectrum and $(\hat{\mathbf{z}}_i(\tilde{f}))^P$ is the estimate of $\mathbf{z}_i(\tilde{f})$ from the p th frame.

The cyclic spectrum recovery processing is presented here in the frequency domain. The reconstruction can be equivalently performed in the time domain by modulating the slices to replace the frequency shift $\tilde{f} + a$. Then, $\hat{\mathbf{r}}_x^\alpha[n]$ can be recovered using the time equivalent of (61). However, the carrier frequencies f_i and bandwidths B_i estimation is performed on the cyclic spectrum, in the frequency domain. Thus, the Fourier transform of $\hat{\mathbf{r}}_x^\alpha[n]$ needs to be computed, and $S_x^\alpha(f)$ is then mapped using (30) for (f, α) defined in (31). Therefore, we choose to perform the whole processing in the frequency domain. Another reason to do so is that SBR2 can obviously be performed in the frequency domain only, as opposed to SBR4 which can be carried out both in time and frequency.

We note that in theory, our approach does not require any discretization, neither in the angular frequency f nor in the cyclic frequency α . Indeed, $\mathbf{R}_x^\alpha(\tilde{f})$ can be computed for any $a \in [0, f_s]$ and $\tilde{f} \in [0, f_s - a]$. This distinguishes our scheme from those based on a transformation between Nyquist and sub-Nyquist samples, where the resolution is theoretically inherent to the problem dimension and dictated by the length of the Nyquist samples vector. In practice, the resolution both in f and α obviously depends on the sensing time and is determined by the number of samples, namely the number of discrete Fourier transform (DFT) coefficients of $\hat{\mathbf{z}}(\tilde{f})$.

We compare our cyclostationary detection to energy detection based on power spectrum recovery, presented in [18]. There, it was shown that power spectrum sensing outperforms spectrum sensing, namely energy detection performed on the recovered signal itself. This power spectrum reconstruction approach is a special case of ours for $a = 0$, when only the matrix $\mathbf{R}_x^0(\tilde{f})$ is considered and only its diagonal is reconstructed. Therefore, we compare our detection approach performed on $S_x^\alpha(f)$ for $\alpha \neq 0$ to energy detection carried out on $S_x^\alpha(f)$, for $\alpha = 0$, corresponding to the diagonal elements of $\mathbf{R}_x^0(f)$.

Throughout the simulations we consider additive white Gaussian noise (AWGN), so that the received signal can be written as

$$y(t) = x(t) + n(t), \quad (63)$$

where $x(t)$ is the wideband signal defined in (1) and $n(t)$ is the wideband AWGN. The SNR is defined as the ratio between the power of the wideband signal and that of the wideband noise as follows

$$\text{SNR} = \frac{\|x(t)\|^2}{\|n(t)\|^2}. \quad (64)$$

B. Cyclic Spectrum Recovery

We first illustrate cyclic spectrum reconstruction from sub-Nyquist samples. We consider $x(t)$ composed of $N_{\text{sig}} = 3$ AM transmissions. Each transmission has bandwidth $B = 80\text{MHz}$ and the carrier frequencies are drawn uniformly at random in $[0, \frac{f_{\text{Nyq}}}{2}]$, with $f_{\text{Nyq}} = 6.4\text{GHz}$. The SNR is set to -5dB . In the sampling stage, we use the MWC with $M = 11$ channels,

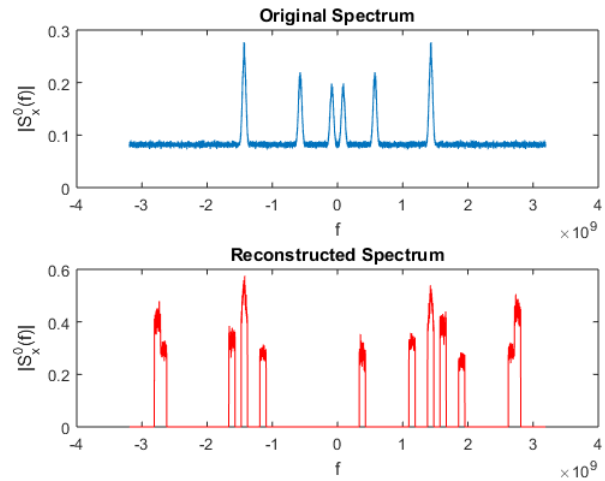


Fig. 5. Original (top) and reconstructed (bottom) power spectrum ($\alpha = 0$).

each sampling at $f_s = 95\text{MHz}$. The overall sampling rate is therefore 1.05GHz , that is 2.2 times the Landau rate and 16% of the Nyquist rate. Here, the theoretical minimal sampling rate is $f_{\text{min}} = 768\text{MHz}$.

Figure 5 shows the original and reconstructed power spectrum of $x(t)$, namely $S_x^0(f)$. In this experiment, the carriers are $f_1 = 97\text{MHz}$, $f_2 = 573\text{MHz}$ and $f_3 = 1.4\text{GHz}$. We observe that the recovery of the power spectrum failed; some occupied bands were not reconstructed and others that only contained noise were identified as active. This is due to the poor performance of energy detection in low SNR regimes. In can be seen in Fig. 5 that the signal spectrum is not buried in noise and the transmissions would have been perfectly detected using energy detection on Nyquist samples. However, in sub-Nyquist regimes, the aliasing decreases the SNR [19], as can be seen in Fig. 6, which shows the DFT of the samples of one channel. As a consequence, energy detection failed in this sub-Nyquist regime.

The reconstructed cyclic spectrum of $x(t)$ is presented in Fig. 7 (the reader is referred to the colored version for a clearer figure), where we observe that the noise contribution is concentrated at $\alpha = 0$ while it is significantly lower at the non zero cyclic frequencies. For clarity, we focus on the one-dimensional section of $S_x^\alpha(f)$ for $f = 0$, shown in Fig. 8. It can be clearly seen that the highest peaks (at least 6dB above the lower peaks) are located at $\alpha_i = 2f_i$ for all 3 active transmissions. This illustrates the advantage of cyclostationary detection in comparison with energy detection.

Next, we perform cyclostationary detection on the reconstructed cyclic spectrum. We use a single-cycle detector which computes the energy at several frequencies around $f = 0$ and at a single cyclic frequency α . In the simulations, we consider AM modulated signals. We address a blind scenario where the carrier frequencies of the signals occupying the wideband channel are unknown and we have $N_{\text{sig}} = 3$ potentially active transmissions, with single-sided bandwidth $B = 100\text{MHz}$.

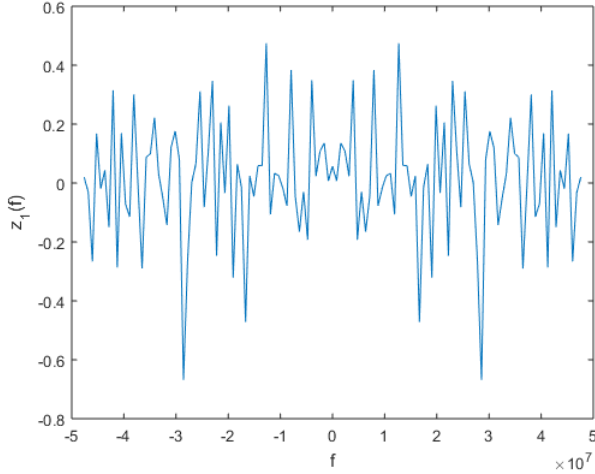


Fig. 6. Sub-Nyquist samples in the first channel in the frequency domain.

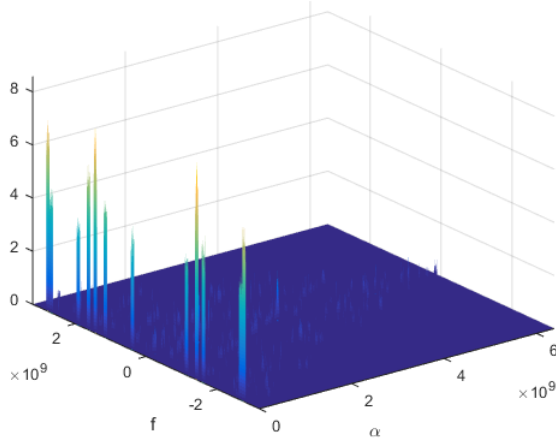


Fig. 7. Reconstructed cyclic spectrum.

The Nyquist rate of $x(t)$ is $f_{\text{Nyq}} = 10\text{GHz}$. We consider $N = 64$ spectral bands and $M = 7$ analog channels, each sampling at $f_s = 156\text{MHz}$. The overall sampling rate is $Mf_s = 1.09\text{MHz}$ which is 182% of the Landau rate and 10.9% of the Nyquist rate. Here, the theoretical minimal sampling rate is $f_{\text{min}} = 960\text{MHz}$. The receiver operating characteristic (ROC) curve is shown in Fig. 9 for different SNR regimes (the averages were performed over $P = 15$ frames).

C. Carrier Frequencies and Bandwidths Recovery

We now demonstrate carrier frequencies and bandwidths estimation from sub-Nyquist samples. We first illustrate our algorithm process on a specific experiment. We consider $x(t)$ composed of $N_{\text{sig}} = 3$ BPSK transmissions, which have cyclic features at the locations $(f, \alpha) = (0, \pm f_c), (\pm f_c, \pm \frac{1}{T})$, where

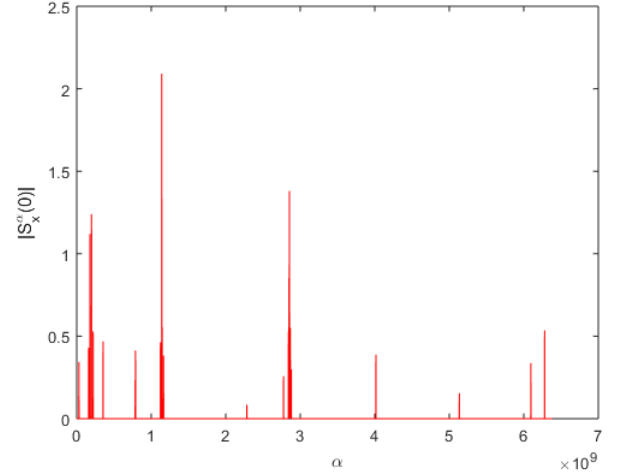


Fig. 8. Reconstructed cyclic spectrum for $f = 0$, $S_x^\alpha(0)$, as a function of the cyclic frequency α .

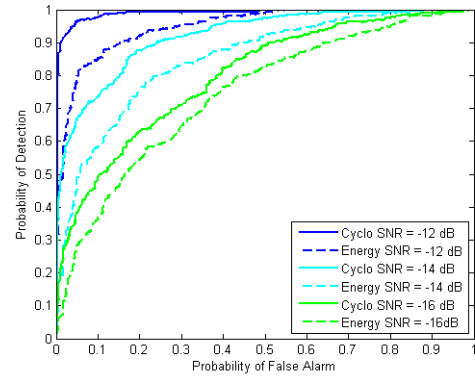


Fig. 9. ROC for both energy and cyclostationary detection.

f_c is the carrier frequency and T is the symbol period [6]. Each transmission has bandwidth $B = 18\text{MHz}$ and the carrier frequencies are drawn uniformly at random in $[0, \frac{f_{\text{Nyq}}}{2}]$, with $f_{\text{Nyq}} = 1\text{GHz}$. In this experiment, the selected carriers are $f_1 = 163.18\text{MHz}$, $f_2 = 209.69\text{MHz}$ and $f_3 = 396.12\text{MHz}$. The SNR is set to -5dB . In the sampling stage, we use the MWC with $M = 9$ channels, each sampling at $f_s = 23.26\text{MHz}$. The overall sampling rate is therefore 210MHz , that is a little below twice the Landau rate and 21% of the Nyquist rate. Here, the theoretical minimal sampling rate is $f_{\text{min}} = 172.8\text{MHz}$.

Figure 10 presents the original and reconstructed power spectrum using $P = 100$ frames. We observe that the signal's spectrum was not perfectly recovered due to the noise. The reconstructed cyclic spectrum, including the power spectrum, estimated over $P = 100$ frames as well, is shown in Fig. 11 and the section corresponding to $f = 0$ can be seen in Fig. 12. The cyclic peaks at the locations $(f, \alpha) = (0, \pm f_i)$, for $i = 1, 2, 3$ can be observed in both figures. In Fig. 13, we

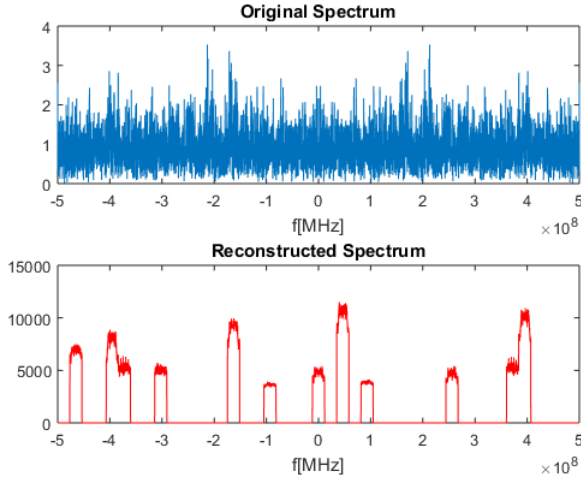


Fig. 10. Original and reconstructed power spectrum.

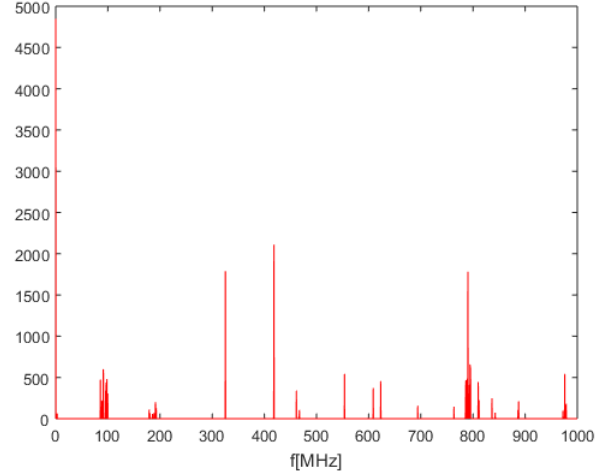


Fig. 12. Reconstructed cyclic spectrum for $f = 0$, $S_x^\alpha(0)$, as a function of the cyclic frequency α .

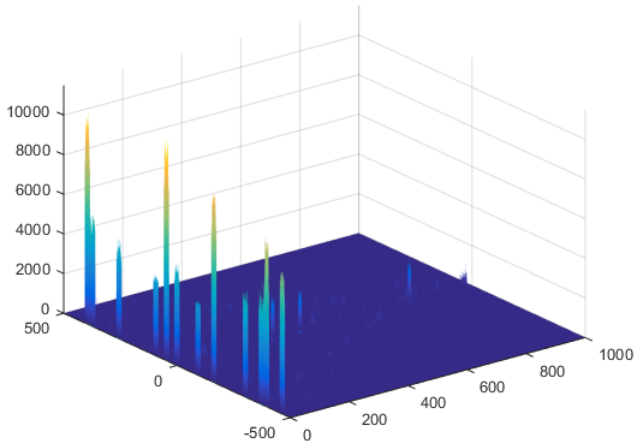


Fig. 11. Reconstructed cyclic spectrum.

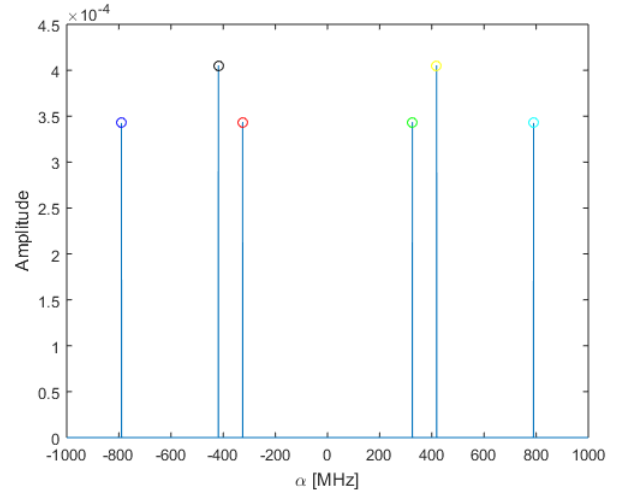


Fig. 13. Clustering with $k = 6$.

illustrate the clustering stage of our algorithm, applied to the cyclic frequency as a function of α for $f = 0$. The estimated number of clusters is 6, yielding an correctly estimated number of signals $\hat{N}_{\text{sig}} = 3$. The estimated carrier frequencies using cyclostationary based estimation are $\hat{f}_1 = 162.66\text{MHz}$, $\hat{f}_2 = 209.19\text{MHz}$ and $\hat{f}_3 = 395.11\text{MHz}$, and the corresponding estimated bandwidths $\hat{B}_1 = 17.4\text{MHz}$, $\hat{B}_2 = 17.4\text{MHz}$ and $\hat{B}_3 = 17.0\text{MHz}$. Using energy based estimation, we obtain $\hat{N}_{\text{sig}} = 5$ signals, with estimated carrier frequencies $\hat{f}_1 = 93.04\text{MHz}$, $\hat{f}_2 = 162.82\text{MHz}$, $\hat{f}_3 = 255.86\text{MHz}$ and $\hat{f}_4 = 383.89\text{MHz}$, $\hat{f}_5 = 465.21\text{MHz}$ and estimated bandwidths $\hat{B}_1 = \hat{B}_2 = \hat{B}_3 = \hat{B}_5 = 23.1\text{MHz}$, $\hat{B}_4 = 46.3\text{MHz}$. Clearly, cyclostationary detection succeeded where energy detection failed.

We now investigate the performance of our carrier frequency

and bandwidth estimation algorithm from sub-Nyquist samples with respect to SNR and compare it to energy detection. We consider $x(t)$ composed of $N_{\text{sig}} = 3$ BPSK transmissions with identical parameters as in the previous section. The sampling parameters remain the same as well. In each experiment, we draw the carrier frequencies uniformly at random and generate the transmissions. The results are averaged over 500 realizations.

Fig. 14 shows the probability of detection of both cyclostationary (blue) and energy (red) detection. A detection is reported if the distance between the true and recovered carrier frequencies is below 10 times the frequency resolution. The average number of false alarms, namely unoccupied bands that are labelled as detection, is shown in Fig. 15. Clearly, cyclostationarity outperforms the energy approach in terms

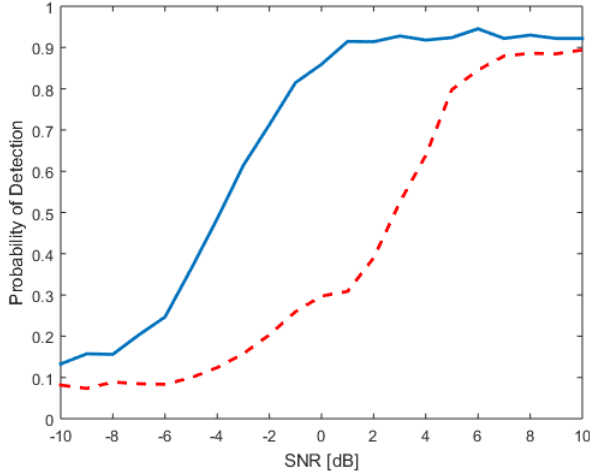


Fig. 14. Probability of detection - cyclostationary vs. energy detection.

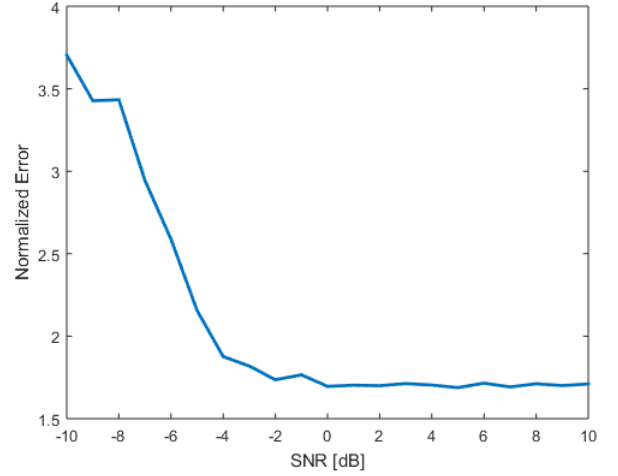


Fig. 16. Normalized carrier frequency recovery error.

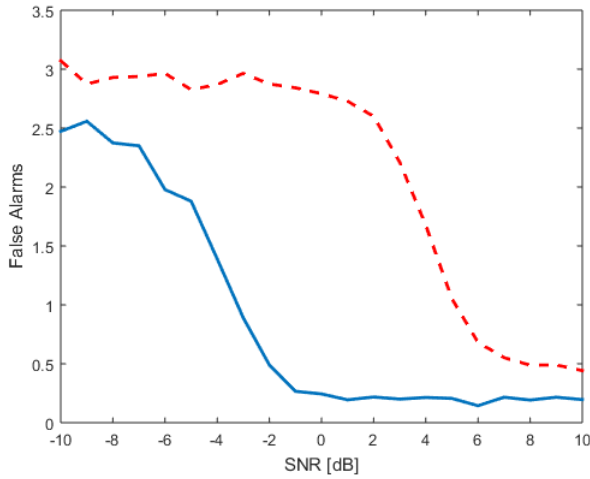


Fig. 15. False alarm - cyclostationary vs. energy detection.

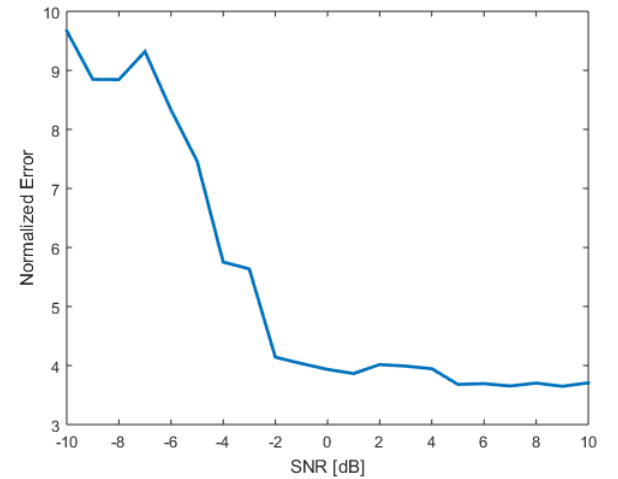


Fig. 17. Normalized bandwidth recovery error.

of probability of detection. Cyclostationary detection also yields less false alarms above a certain SNR level. The carrier frequencies and bandwidths reconstruction errors are presented in Figs. 16 and 17, respectively. It can be seen that, above a certain SNR level, -2 dB in these settings, the recovery errors do not increase with SNR decrease.

VI. CONCLUSION

In this paper, we considered cyclostationary detection at a sub-Nyquist regime, to cope with efficiency and robustness requirements for spectrum sensing in the context of CR. We presented a cyclic spectrum reconstruction algorithm from sub-Nyquist samples along with recovery conditions for both the sparse and non sparse case. We showed that even if the signal is not sparse, its cyclic spectrum can be recovered from samples obtained below the Nyquist rate. The minimal

rates obtained from both the sparse and non sparse cases are found to be higher than those required for power spectrum recovery only and lower than the rates required for signal reconstruction. Once the cyclic spectrum is recovered, we applied our feature extraction algorithm that estimates the number of transmissions and their respective carrier frequency and bandwidth. Simulations performed at low SNRs validate that cyclostationary detection outperforms energy detection in the sub-Nyquist regime.

REFERENCES

- [1] H. Urkowitz, "Energy detection of unknown deterministic signals," *Proceedings of the IEEE*, vol. 55, pp. 523–531, Apr. 1967.
- [2] D. O. North, "An analysis of the factors which determine signal/noise discrimination in pulsed carrier systems," *Proceedings of the IEEE*, vol. 51, pp. 1016–1027, Jul. 1963.

- [3] G. L. Turin, "An introduction to matched filters," *IRE Trans. on Information Theory*, vol. 6, pp. 311–329, Jun. 1960.
- [4] W. A. Gardner, A. Napolitano, and L. Paura, "Cyclostationarity: Half a century of research," pp. 639–697, 2006.
- [5] A. Napolitano, "Cyclostationary: New trends and applications," *Signal Process.*, vol. 120, pp. 385–408, Jan. 2016.
- [6] W. Gardner, *Statistical spectral analysis: a non probabilistic theory*. Prentice Hall, 1988.
- [7] J. Mitola, "Software radios: Survey, critical evaluation and future directions," *IEEE Aerosp. Electron. Syst. Mag.*, vol. 8, pp. 25–36, Apr. 1993.
- [8] E. Axell, G. Leus, E. Larsson, and H. Poor, "Spectrum sensing for cognitive radios: State-of-the-art and recent advances," *IEEE Signal Process. Magazine*, vol. 29, pp. 101–116, May 2012.
- [9] FCC, "Spectrum policy task force report: Federal communications commission, tech. rep. 02-135. [online]," http://www.gov/edocs_public/attachmatch/DOC228542A1.pdf, Nov. 2002.
- [10] M. McHenry, "NSF spectrum occupancy measurements project summary. shared spectrum co., tech. rep. [online]," <http://www.sharedspectrum.com>, Aug. 2005.
- [11] R. I. C. Chiang, G. B. Rowe, and K. W. Sowerby, "A quantitative analysis of spectral occupancy measurements for cognitive radio," *IEEE Vehicular Technology Conf.*, pp. 3016–3020, Apr. 2007.
- [12] M. Mishali and Y. C. Eldar, "Blind multi-band signal reconstruction: Compressed sensing for analog signals," *IEEE Trans. on Signal Process.*, vol. 57, no. 3, pp. 993–1009, Mar. 2009.
- [13] —, "From theory to practice: Sub-Nyquist sampling of sparse wideband analog signals," *IEEE J. Sel. Topics Signal Process.*, vol. 4, no. 2, pp. 375–391, Apr. 2010.
- [14] —, "Sub-Nyquist sampling: Bridging theory and practice," *IEEE Signal Proc. Magazine*, vol. 28, no. 6, pp. 98–124, Nov. 2011.
- [15] Y. C. Eldar, *Sampling Theory: Beyond Bandlimited Systems*. Cambridge University Press, 2015.
- [16] M. A. Lexa, M. E. Davies, J. S. Thompson, and J. Nikolic, "Compressive power spectral density estimation," *IEEE ICASSP*, vol. 57, pp. 22–27, May 2011.
- [17] D. D. Ariananda and G. Leus, "Compressive wideband power spectrum estimation," *IEEE Trans. on Signal Process.*, vol. 60, pp. 4775–4789, Sept. 2012.
- [18] D. Cohen and Y. C. Eldar, "Sub-Nyquist sampling for power spectrum sensing in cognitive radios: A unified approach," *IEEE Trans. on Signal Process.*, vol. 62, pp. 3897–3910, Aug. 2014.
- [19] E. Arias-Castro and Y. C. Eldar, "Noise folding in compressed sensing," *IEEE Signal Process. Letters*, vol. 18, no. 8, pp. 478–481, Aug. 2011.
- [20] C. M. Spooner and R. B. Nicholls, *Spectrum sensing based on spectral correlation*, in: B. Fette (Ed.), *Cognitive Radio Technology, 2nd ed. (Chapter 18)*. Elsevier, 1909.
- [21] S. Haykin, D. J. Thomson, and J. H. Reed, "Spectrum sensing for cognitive radio," *Proceedings of the IEEE*, vol. 97, pp. 849–877, 2009.
- [22] E. Rebeiz, V. Jain, and D. Cabric, "Cyclostationarity-based low complexity wideband spectrum sensing using compressive sampling," in *IEEE ICC*, Jun. 2012, pp. 1619–1623.
- [23] Z. Khalaf, A. Nafkha, and J. Palicot, "Blind cyclostationary feature detector based on sparsity hypotheses for cognitive radio equipment," *IEEE MWSCAS*, pp. 1–4, 2011.
- [24] —, "Blind spectrum detector for cognitive radio using compressive sensing," *IEEE GLOBECOM*, pp. 1–5, 2011.
- [25] Z. Tian, "Cyclic feature based wideband spectrum sensing using compressive sampling," *IEEE ICC*, pp. 1–5, Jun. 2011.
- [26] Z. Tian, Y. Tafesse, and B. M. Sadler, "Cyclic feature detection with sub-nyquist sampling for wideband spectrum sensing," *IEEE Journal on Sel. Topics Signal Process.*, vol. 6, no. 1, pp. 58–69, Feb. 2012.
- [27] S. A. Razavi, M. Valkama, and D. Cabric, "High-resolution cyclic spectrum reconstruction from sub-Nyquist samples," *IEEE SPAWC*, pp. 250–254, Jun. 2013.
- [28] G. Leus and Z. Tian, "Recovering second-order statistics from compressive measurements," *IEEE CAMSAP*, pp. 337–340, Dec. 2011.
- [29] D. D. Ariananda and G. Leus, "Non-uniform sampling for compressive cyclic spectrum reconstruction," *IEEE ICASSP*, pp. 41–45, 2014.
- [30] L. Zhu, C. E. Luo, and J. H. McClellan, "Cyclostationary-based wideband spectrum sensing using random sampling," *IEEE GlobalSIP*, pp. 1202–1205, 2013.
- [31] Y. C. Eldar and G. Kutyniok, *Compressed Sensing: Theory and Applications*. Cambridge University Press, 2012.
- [32] C. E. Luo and J. H. McClellan, "Compressive sampling with a successive approximation ADC architecture," *IEEE ICASSP*, pp. 3920–3923, May 2011.
- [33] M. Mishali, Y. C. Eldar, O. Dounaevsky, and E. Shoshan, "Xampling: Analog to digital at sub-nyquist rates," *IET Circuits, Devices & Systems*, vol. 5, no. 1, pp. 8–20, Jan. 2011.
- [34] D. Cohen, L. Pollak, and Y. C. Eldar, "Carrier frequency and bandwidth estimation of cyclostationary multiband signals," *IEEE ICASSP*, Mar. 2016.
- [35] J. R. Barry, E. A. Lee, and D. G. Messerschmitt, *Digital Communication*. Springer, 2003.
- [36] A. Papoulis, *Probability, Random Variables, and Stochastic Processes*. McGraw Hill, 1991.
- [37] R. Venkataramani and Y. Bresler, "Perfect reconstruction formulas and bounds on aliasing error in sub-Nyquist nonuniform sampling of multiband signals," *IEEE Trans. Inf. Theory*, vol. 46, pp. 2173 – 2183, Sept. 2000.
- [38] R. L. Thorndike, "Who belong in the family?" *Psychometrika*, vol. 18, pp. 267–276, Dec. 1953.